

Article

Cladding-Pumped Er/Yb-Co-Doped Fiber Amplifier for Multi-Channel Operation

Kaspars Zakis ^{1,2,*}, Sergejs Olonkins ³, Aleksejs Udalcovs ¹, Ingars Lukosevics ⁴, Dmitrijs Prigunovs ^{1,3}, Jurgis Grube ⁴, Liga Bikse ⁴, Andis Supe ¹, Oskars Ozolins ¹, Sandis Spolitis ^{1,2} and Vjaceslavs Bobrovs ¹

- ¹ Institute of Telecommunications, Riga Technical University, LV-1048 Riga, Latvia; aleksejs.udalcovs@gmail.com (A.U.); dmitrijs.prigunovs@rtu.lv (D.P.); andis.supe@rtu.lv (A.S.); oskars.ozolins@rtu.lv (O.O.); sandis.spolitis@rtu.lv (S.S.); vjaceslavs.bobrovs@rtu.lv (V.B.)
- ² Communication Technologies Research Center, Riga Technical University, LV-1048 Riga, Latvia
- ³ AFFOC Solutions, LV-3016 Kalnciems, Latvia; sergejs.olonkins@rtu.lv
- ⁴ Institute of Solid State Physics, University of Latvia, LV-1063 Riga, Latvia; ingars.lukosevics@cfi.lu.lv (I.L.); jurgis.grube@cfi.lu.lv (J.G.); liga.bikse@cfi.lu.lv (L.B.)
- * Correspondence: kaspars.zakis@rtu.lv

Abstract: Cladding-pumped erbium (Er³⁺)/ytterbium (Yb³⁺)-co-doped fiber amplifiers are more advantageous at high output powers. However, this amplification technique also has potential in telecom-related applications. These types of amplifiers have complex properties, especially when considering gain profile and a pump conversion efficiency. Such metrics depend on the doped fiber profile, absorption/emission spectra, and the input signal power. In this context, we design, build and characterize an inhouse prototype of cladding-pumped Er³⁺/Yb³⁺-co-doped fiber amplifier (EYDFA). Our goal is to identify the EYDFA configuration (a co-doped fiber length, pump power, input signal power) suitable for signal amplification in a multichannel fiber-optic transmission system with a dense wavelength allocation across the C-band (1530–1565 nm). Our approach involves experimentally determining the Er³⁺/Yb³⁺-co-doped fiber's parameters to be used in a simulation setup to decide on an initial EYDFA configuration before moving to a laboratory setup. An experimental EYDFA prototype is tested under different conditions using a 48-channel dense wavelength division multiplexing (DWDM, 100 GHz) system to evaluate the absolute gain and gain uniformity. The obtained results allow the cladding pump amplifier's suitability for wideband signal amplification to be assessed. The developed prototype provides > 21 dB of gain with a 12 dB ripple within 1534–1565 nm. Furthermore, we show that the gain profile can be partially flattened out by using longer EYDF spans. This enhances signal amplification in the upper C-band in exchange for a weaker amplification in the lower C-band, which can be marginally improved with higher pump powers.

Keywords: absorption and emission spectra; cladding-pumped doped fiber amplifier; erbium/ytterbium co-doping; fiber-optic systems; overlap factor; wavelength division multiplexing

Citation: Zakis, K.; Olonkins, S.; Udalcovs, A.; Lukosevics, I.; Prigunovs, D.; Grube, J.; Bikse, L.; Supe, A.; Ozolins, O.; Spolitis, S.; et al. Cladding-Pumped Er/Yb-Co-Doped Fiber Amplifier for Multi-Channel Operation. *Photonics* **2022**, *9*, 457. <https://doi.org/10.3390/photonics9070457>

Received: 10 June 2022

Accepted: 26 June 2022

Published: 28 June 2022

Publisher's Note: MDPI stays neutral with regard to jurisdictional claims in published maps and institutional affiliations.



Copyright: © 2022 by the authors. Licensee MDPI, Basel, Switzerland. This article is an open access article distributed under the terms and conditions of the Creative Commons Attribution (CC BY) license (<https://creativecommons.org/licenses/by/4.0/>).

1. Introduction

Cladding-pumped erbium (Er³⁺)/ytterbium (Yb³⁺)-co-doped amplifiers are typically associated with high-power laser systems and their applications. However, telecom-related applications have also gained momentum by proving their particular significance in such applications. The multifold of different fiber structures and techniques can be designed to address specific telecom amplifier needs, for instance, a multi-cladding optical fiber with a non-circular symmetry that aims to enhance pump absorption via twisting and coiling [1], the reduction in nonlinear effects with tapered fiber [2], fiber dispersion engineering [3,4]. The simulation of cladding-pumped doped fiber amplifier performance is also of particular interest due to the necessity of obtaining initial estimates of the key

performance indicators, such as noise figure (NF) and gain [5]. The cladding pumping technique is more advantageous over core pumping amplifiers at high output powers (typically > 100 mW). Additionally, in the case of cladding-pumping, Er³⁺/Yb³⁺ co-doping (compared to pure Er³⁺ doping) allows for significantly improved pump utilization and reduced noise figure, especially at higher input power. The noise figure is expected to be <5 dB (comparable to typical core-pumped EDFAs), increasing above 1545 nm with higher pump power [6].

Commercial single-core erbium (Er³⁺)/ytterbium (Yb³⁺)-co-doped fiber amplifiers for C-band operation typically cover the wavelength range between 1540–1560 nm (± 5 nm), a reduction in bandwidth compared to typical erbium (Er³⁺) doped fiber amplifiers. However, detailed information on amplifier gain and NF wavelength dependence as a function of signal and/or pump power, are normally not included in technical data sheets. It is also difficult to carry out a fair comparison between amplifiers of different manufacturers since the used pumping scheme, core or cladding, is unknown. The technique used may be inferred from the typical output power and pump current values if such data are provided.

In this paper, we describe an Er³⁺/Yb³⁺-co-doped fiber amplifier (EYDFA) suitable for telecom applications (signal gain around 30 dB and output power up to 23 dBm). Our goal is to explore the wavelength dependence of the amplifier's gain based on EYDF length, input signal and pump power. For a complete understanding of the amplifier's gain evolution within the fibers, a series of measurements were performed with a wideband multi-channel input signal. EYDFA testing was conducted by amplifying a 48-channel dense wavelength division multiplexed (DWDM) signal on a 100 GHz frequency grid that covers the entire C-band.

The rest of the paper is organized as follows. Section 2 describes the experimental extraction of the EYDF characteristics (specifically, Er³⁺ and Yb³⁺ absorption and emission cross-sections and overlap coefficient) required for finetuning the EYDFA simulation setup. The simulation and experimental setups used to characterize the EYDFA's performance are given in Section 3. In Section 4, we present the experimental results, characterizing the performance of our in-house cladding-pumped EYDFA. Finally, Section 5 concludes the paper.

2. Characterization of the Erbium/Ytterbium-Co-Doped Fiber Parameters

Part of our research is devoted to the validation of the previously developed cladding-pumped EYDFA simulation model (see the description in Section 3 and [5]). The laboratory setup is used to fine-tune the simulation model, the accuracy of which is primarily determined by the double-clad EYDF parameters, being the gain medium. The simulation model uses EYDF's absorption and emission cross-sections and the so-called overlap factor [5]. The dopant ion cross-section is calculated based on absorption spectra measurements and other parameters, such as dopant ion concentrations, fiber core and cladding refractive indices. Manufacturers typically do not provide information on these doped fiber properties. Accordingly, this section gives a more detailed description of all the experimental setups used to obtain the missing physical parameters of the EYDF: (a) Er³⁺ and Yb³⁺ concentrations, (b) core and inner cladding overlap factor, (c) refractive index profile, and (d) Er³⁺/Yb³⁺ absorption and emission spectra and cross-sections [7,8]. The fiber under test is an Er³⁺/Yb³⁺-co-doped double-clad fiber that has a flower-shaped inner cladding, which is discussed further in section 2.2..

2.1. Doped Fiber Elemental Analysis

Elemental analysis for the selected double-clad EYDF cross-section was carried out using scanning electron microscopy (SEM) to determine the dopant ion concentrations in the doped fiber's core. Thermo Scientific Helios UX 5 equipped with Energy Dispersive X-ray Spectroscopy (EDS) detector was used for the measurements. The EDS point ID was measured at 15 kV and 0.40 nA for a live time of 300 s. The EYDF sample was covered

with a thin 30 nm gold layer to detect elemental distribution in the cross-section without causing a surface-charging effect. The line scan was measured at 125 points along the diameter of the EYDF. The measurement time was approximately half an hour with beam parameters 20 kV and 0.40 nA. Elemental quantification of the spectra was carried out using Pathfinder X-ray Microanalysis Software [9]. The elemental composition of the fiber core was analyzed in terms of the atomic percentage (at%) of one kind of atom relative to the total atoms in the sample and resulted in the following values: 61.71% O, 30.98% Si, 6.04% P, 0.06% Er and 1.21% Yb. However, for the EDS line scan across the diameter of the fiber, it was covered with a thin gold layer, and the calculated elemental distribution was not corrected with respect to Au layer absorption. Nevertheless, Figure 1 clearly shows that in the core regions Yb, P, and Er replace some part of the Si atoms and that fluorine is located at the edge of the fiber in an approximately 10 μm -wide ring—the second cladding. In the case of fluorine, it replaces oxygen atoms in the outer shell. Phosphorus in the fiber core increases the silica fiber refractive index. The inner cladding consists of pure silica without any traces of rare-earth or other dopant elements. The outer cladding consists of silica doped with fluorine to reduce the material refractive index.

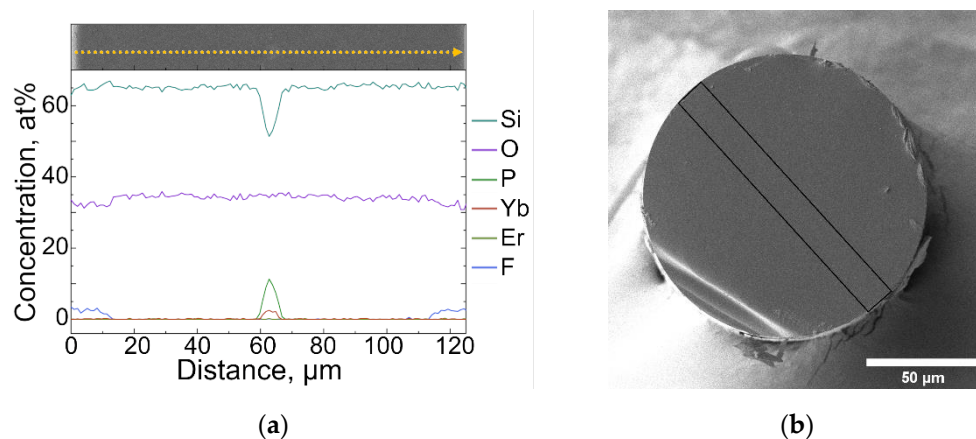


Figure 1. (a) EDS line scan represented by the yellow dotted line with the corresponding elemental distribution underneath; (b) EYDF cross-section where the black rectangle is the EDS line scan region.

For the amplification processes, the concentration of the rare-earth elements in the core is important. The EDS measurements show that Yb^{3+} and Er^{3+} concentrations are 1.21 at% and 0.06 at%, respectively. Consequently, the Yb^{3+} to Er^{3+} ratio is 20.17, which is close to the EYDF datasheet specification of 20. The experimentally obtained dopant ion concentration values were used to calculate absorption/emission cross-section areas (see Section 2.4).

2.2. Overlap Factor Calculation

To increase pumping efficiency, the inner cladding of double-clad doped optical fiber is often formed into a specific shape (e.g., star-shape [10], D-shape [11], flower-shaped [12], etc.). This improves pump absorption by supporting modal regimes that focus pump light toward the doped fiber's core. The waveguide geometry of a double-clad fiber in the simulation model is represented using the so-called overlap factor. The overlap factor is defined as the following ratio:

$$\Gamma = \frac{A_c}{A_{icl}} \quad (1)$$

where Γ is the overlap factor, A_c is the core area, and A_{icl} is the inner cladding area [10].

Fiber manufacturers tend to only provide overall geometrical dimensions without specifically providing core or inner-cladding areas. Accordingly, the estimation of A_c and

A_{id} becomes a task in itself. The overlap factor was obtained by analyzing the EYDF cross-section image, as shown in Figure 2a.

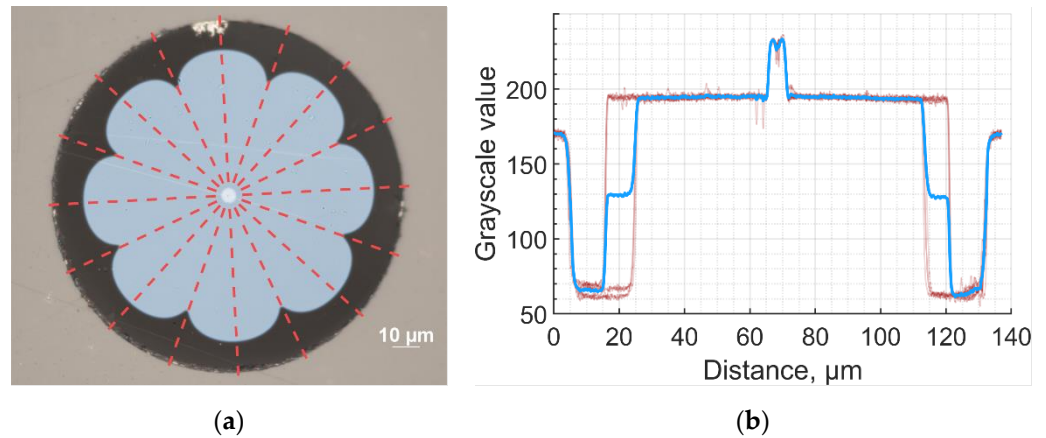


Figure 2. (a) Double-clad EYDF cross section; (b) the resulting line profiles in red with their average shown in blue.

The fiber’s cross-section in the visible spectral range is measured using the Eclipse LV150N microscope [13] with the Plan FLUOR BD objective lens from Nikon [14] coupled with the DS-Fi3, 5.9 Mpixel (2880 × 2048) camera [15]. A total of eight different crossings were selected from the cross-section image (see red dashed lines in Figure 2) all crossing the center. Measurements (pixel grayscale values versus diameter) are averaged to minimize image noise, as well as to account for the fiber’s imperfections, as shown in Figure 2b. Using this approach, four regions can be distinguished—two outer/inner cladding boundaries and two inner cladding/core boundaries. The exact position of the boundaries is calculated by fitting each transition region with a separate sigmoid function as described in [16]:

$$Z(x) = \frac{A}{1 + e^{c(x-x_0)}} + B, \tag{2}$$

where:

$Z(x)$ fiber profile;

x position;

A, B, c sigmoid function fitting coefficients;

x_0 edge of the boundary.

We obtained the overlap factor value of 0.0027 and outer cladding diameter of 127.03 ± 0.01 μm, which is around 2 μm larger than the measurement of 125 μm specified by the manufacturer.

2.3. Refractive Index

The fiber’s core and cladding refractive indices are needed as inputs for absorption and emission cross-section calculations. Measurements of the refractive index difference can be seen in Figure 3.

The difference between the core and the first cladding is $n_1 - n_2 = 0.0138 \pm 0.0003$, and the difference between the first cladding and the second cladding is $n_2 - n_3 = 0.0239 \pm 0.0003$ at the wavelength of 633 nm. A reference value is required to calculate the absolute values of each refractive index. We suppose that the most robust reference, in this case, would be the inner cladding consisting of pure silica. The composition of this region was verified using an SEM elemental analysis, and it was found that the composition was most likely SiO_{1.9}. With this information and by referencing [17], we calculated the following refractive index values:

- Outer cladding $n_3 = 1.505 \pm 0.004$;
- Inner cladding $n_2 = 1.529 \pm 0.004$;
- Core $n_1 = 1.543 \pm 0.004$.

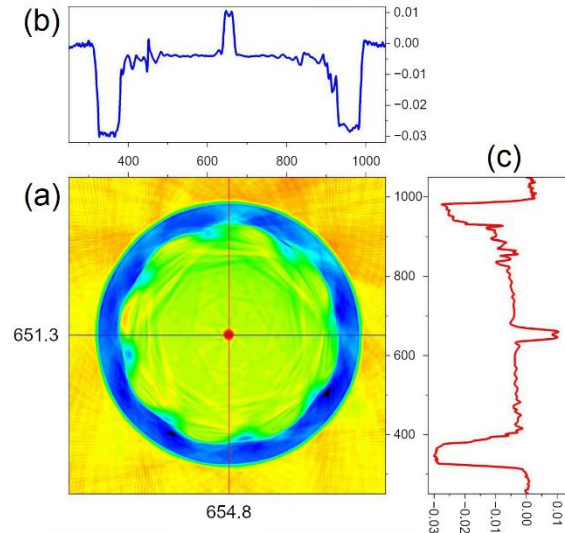


Figure 3. (a) EYDF cross-section refractive index difference measurements: (b) along the horizontal axis, (c) along the vertical axis.

2.4. Absorption and Emission Cross-Section

To estimate the EYDF's absorption and emission cross-sections, we obtained the absorption spectra. The absorption spectra measurements were performed using a measurement setup consisting of Agilent's Cary 7000 Universal Measurement Spectrophotometer [18] coupled with the FiberMate2™ Fiber Optic Coupler system from Harrick Scientific Products Inc [19]. The step size was set to 1 nm and spectral bandwidth to 5 nm to obtain an appropriate signal intensity.

An EYDF absorption cross-section was calculated from Er^{3+} and Yb^{3+} absorption spectra using two EYDF samples of different lengths. A 1 m-long EYDF sample was used to perform the absorption spectra measurements around 975 nm wavelength, whereas a 19 m-long sample was used for wavelengths around 1550 nm. In such a way, we avoided the saturation effect that can distort the absorption spectra measurements. The absorption around 975 nm was attributed to the optical transition of Yb^{3+} : ${}^2F_{7/2} \rightarrow {}^2F_{5/2}$ and Er^{3+} : ${}^4I_{15/2} \rightarrow {}^4I_{11/2}$. Nonetheless, the impact of Er^{3+} on absorption in the 975 nm spectral range can be neglected since its absorption cross-section is significantly lower than for Yb^{3+} [20]. Furthermore, according to the previously mentioned concentration measurements, the EYDF has a 20 times higher Yb^{3+} concentration compared to the Er^{3+} concentration, further reducing the Er^{3+} absorption impact in the spectral region centered around 975 nm. Absorption around 1550 nm is attributed to Er^{3+} transition ${}^4I_{15/2} \rightarrow {}^4I_{13/2}$ because Yb^{3+} does not have absorption bands, other than ${}^2F_{7/2} \rightarrow {}^2F_{5/2}$, in the infrared spectral region.

Finally, the absorption cross-section of Er^{3+} and Yb^{3+} was estimated using the measured absorption spectra, overlap factor, length, and $\text{Yb}^{3+}/\text{Er}^{3+}$ concentrations. The emission cross-section was estimated using the McCumber relation [21], which is related to rare-earth element emission and absorption. The output of this calculation is given in Figure 4.

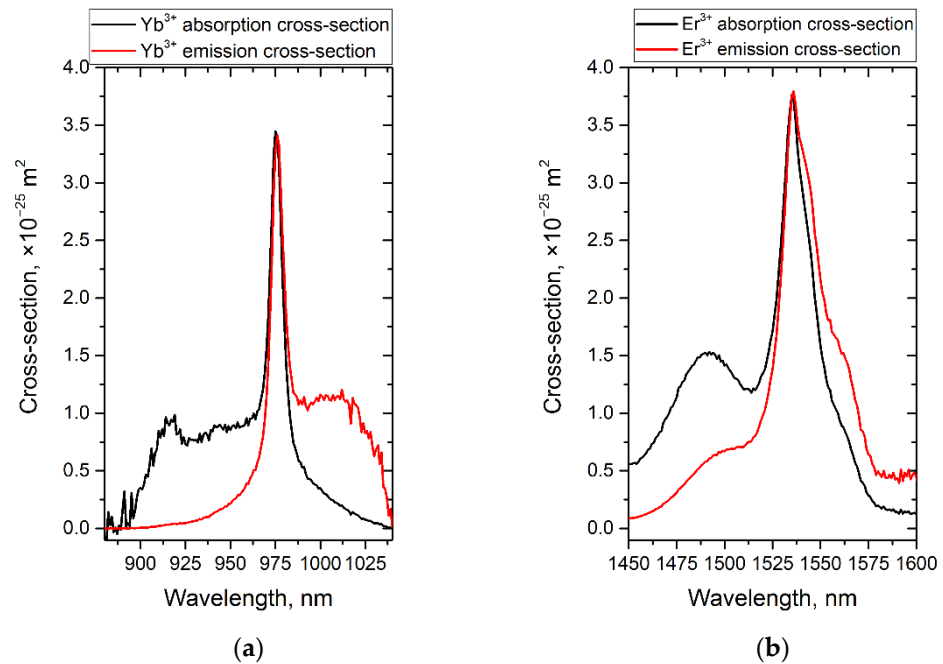


Figure 4. Absorption and emission cross-section spectra calculated from absorption measurements and other parameters for (a) Yb³⁺ and (b) Er³⁺.

3. Amplifier Model and Setup

Cladding-pumped EYDFAs have the potential to be used as booster amplifiers for metro-access networks operating in the optical C-band (1530–1565 nm). DWDM signal allocation is typical for these types of networks. Accordingly, the first step is to create a wideband multichannel signal for testing the amplifier’s performance. In our case, we use a 48-channel signal with 100 GHz channel spacing at −20 dBm per channel (dBm/ch) fully covering the entire C-band.

This section is divided into two subsections where, first, we describe the simulation model that we use to estimate the expected key performance indicators over a range of fiber lengths and, second, we describe the experimental setup of the amplifier under test.

3.1. Simulation Setup

The experimentally obtained EYDF emission and absorption cross-sections and the calculated overlap factor are used as input parameters in the simulation setup of the cladding-pumped EYDFA. This simulation setup is built using VPIphotonics Design Suite [22]; its simplified diagram is shown in Figure 5. The input signal is represented using the experimentally measured spectrum of the 48-channel DWDM signal (see the description in Section 3.2). The main purpose of the simulations is to determine the gain characteristics and provide baseline values of the EYDF length and pump parameters for the experimental setup. Our model from [5] was further improved after measuring the gain of a 3 m-long fiber using the laboratory setup shown in Figure 6.

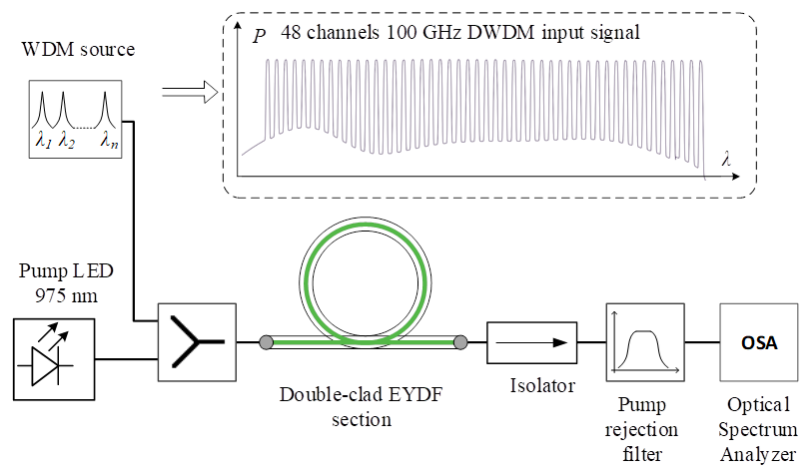


Figure 5. Simplified simulation setup of the cladding-pumped EYDFA.

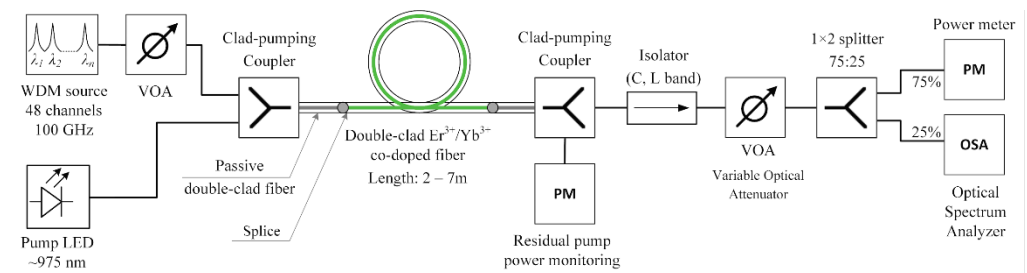


Figure 6. Simplified experimental setup of the cladding-pumped EYDFA. Amplifier’s optical section is between two clad-pumping fiber couplers.

The revised model was then used to estimate the optimal EYDF length and pump power for a wideband signal amplification used in the further measurements that are analyzed in the Results section. The model is based on bidirectional signal propagation equations and multilevel rate equations for ion populations [23,24]. It is resolved in both the longitudinal and transverse directions considering several effects, such as $\text{Er}^{3+}/\text{Yb}^{3+}$ energy transfer, Rayleigh scattering, Kerr nonlinearity, excited-state absorption, and cross-relaxation effects [23]. The main parameters of the EYDF used in the simulations are summarized in Table 1. The EYDF output optical signal is sent through an optical isolator and a band-pass optical filter having a trapezoid-type transfer function (193.75 THz center frequency and 5 THz bandwidth) to filter out any residual pump light before obtaining the output amplified signal spectrum.

Table 1. Amplifier test setup parameters.

System parameters	
Number of channels	48
Channels carrier frequency range	191.35–196.05 THz
Channel spacing	100 GHz
Single-channel power (simulation)	−20 dBm
Single-channel power (experimental)	−25 to −10 dBm
EYDFA pump parameters	
Pump wavelength	973–977 nm at 30 °C
Pump power	0.6–2.5 W
Pumping direction	Co-propagating
Doped fiber parameters	
Length	2–7 m

Er ³⁺ concentration	$1 \times 10^{25} \text{ m}^{-3}$
Yb ³⁺ concentration	$2 \times 10^{26} \text{ m}^{-3}$
Er ³⁺ /Yb ³⁺ cross-relaxation coefficient	$1 \times 10^{-22} \text{ m}^3/\text{s}$
Overlap factor (at 1530 nm)	0.0027
Overlap factor (at 980 nm)	0.9203

3.2. Experimental Setup

To assess the per-channel gain of the experimental EYDFA, we used the input signal that was constructed by filtering a wideband ASE noise source (covering C and L optical bands with a -10 dB bandwidth of 1526–1630 nm) using a wavelength-selective switch (WSS). The WSS has a granularity of 12.5 GHz and a bandwidth of 4.825 THz. Accordingly, a dummy (data-unmodulated wavelengths) WDM signal, consisting of 48 channels that are each 37.5 GHz in bandwidth and located 100 GHz apart from each other, was obtained and is shown in the inset of Figure 5. As the pump source, a high-power multi-mode diode stabilized at 30 °C with a 6 nm bandwidth using a thermoelectric cooler was used in the setup (see Figure 6).

The minimum output power threshold of this pump source is 0.6 W. The active temperature control is important for this diode since, at higher temperatures, the output power decreases, and the spectrum shifts towards longer wavelengths. It was found that keeping the diode’s temperature lower resulted in higher EYDFA gain rather than being closer to the EYDF peak absorption wavelength (976 nm). The pump diode spectrum was centered around 975 nm, which is ~1 nm below the EYDF peak absorption wavelength.

Clad-pumping fiber couplers were connected to both ends of the EYDF. They were used to couple the signal and the pump into double-clad fiber and then to separate the signal from the residual pump, respectively. Optical power at the EYDF output was monitored for both the pump and the DWDM signal. Finally, the spectrum of the output signal was analyzed to obtain the per-channel gain.

4. Results and Discussion

In this section, we present and analyze the results obtained using the previously described simulation and experimental setups. First, we describe our observations related to spontaneous emission emergence. Subsequently, we analyze the amplifier’s gain at different pump power levels and EYDF lengths using experimental and numerical simulations results, revealing the performance of our in-house cladding-pumped EYDFA.

During the initial phase of working with the experimental EYDFA setup (ASE noise measurements and single-channel amplification), it was observed that the amplifier tends to amplify ASE noise, and thus produces stochastic peaks at the output spectrum. Under certain conditions, our EYDFA acted as an unstable laser; therefore, this aspect is studied more in detail. Optical spectra measured for the EYDFA configuration with no input signal are captured in Figure 7.

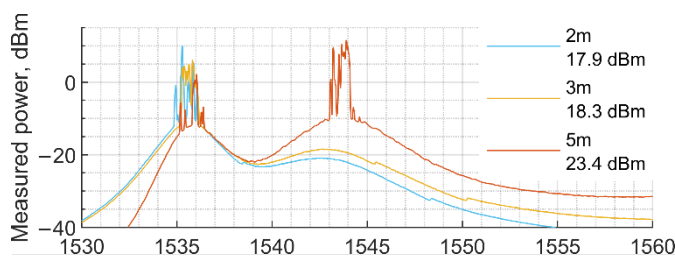


Figure 7. Optical spectra measured for the EYDFA configuration with no input signal with a pump power of 2 W. Lasing is seen that is temporally unstable both in wavelength (within 1 nm) and peak power.

Here, unstable lasing can be observed with no input signal. In the case of the 2 m and 3 m short EYDF spans, lasing is observed around 1536 nm (corresponding to Er^{3+} emission peak; see Figure 4) when the pump power approaches 0.6 W, which corresponds to the threshold current of the pump source. For the 5 m-long EYDF span, we do not observe lasing at 1536 nm; instead, lasing happens around 1544 nm. With the pump power increased to 2 W, we observed a significantly higher lasing at 1544 nm and some (minor) lasing at 1536 nm. Increasing the EYDF length resulted in a more uniform gain profile in the 1544–1565 nm region, as well as a gradual reabsorption of the emission at 1536 nm. The intensity of the observed lasing is proportional to the EYDF length. Yet, it can be mitigated using a sufficiently powerful C-band signal and a power splitter to dump the excess pump light (see Figure 6). It is likely that a laser cavity within the EYDFA is formed due to reflections from connectors, which eventually produces a pulsating laser. It is possible that, with these measurements, we observe the starting phase of a random fiber laser that was demonstrated in [25,26] for cladding-pumped EYDF at similar pump power levels.

The simulation results summarizing the EYDFA gain characteristics are given in Figure 8. It is shown that increasing the EYDF’s length results in the output gain increase in the 1535–1545 nm region, but the gain peak shifts towards longer wavelengths. The corresponding gain values are summarized in Table 2. Such a significant increase is not observed in other wavelength regions of the gain spectrum, i.e., the gain profile is uneven. For instance, at 2 W pump power when the EYDF’s length is increased from 3 to 5 m, an additional 5 dB is gained in the range between 1555 and 1565 nm, and an additional 2.8 dB is gained if the EYDF’s length is further increased to 7 m.

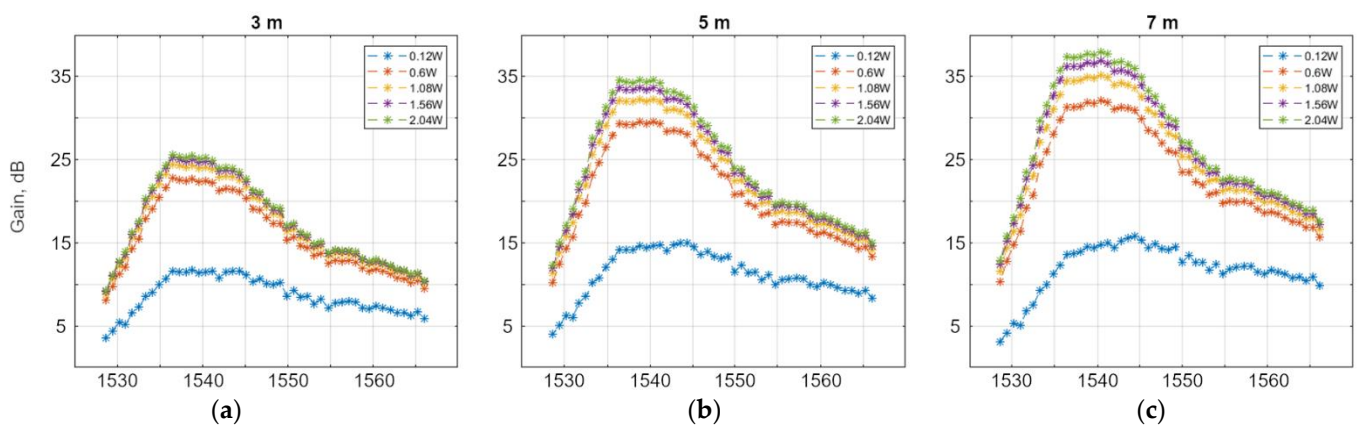


Figure 8. Simulation results showing the EYDFA gain for a -20 dBm/ch 48-channel signal depending on the pump power (0.12–2 W) at three EYDF lengths: (a) 3 m, (b) 5 m and (c) 7 m.

Table 2. Simulated EYDFA gain evolution.

EYDF length, m	3	5	7
Gain max., dB	25.6	34.6	38
Peak gain wavelength, nm	1536.4	1538.8	1540.4
Δ Gain, dB	-	9.1	3.4

Our simulations also show that, in the case of a 3 m-long EYDF, the amplifier produces gain spectra that are almost identical at 1 W and 2 W pump powers. This means that, for relatively short EYDF spans, 1 W of pump power is enough to ensure excited Er^{3+} population inversion to maintain signal amplification. Consequently, using pump powers above 1 W can be considered excessive for such short doped fiber spans. For example, in the case of the 3 m-long EYDF, increasing the pump power from 1 W to 2 W gives only 0.8 dB of additional gain. However, longer EYDF spans provide a larger gain increase (2.3 dB and 2.8 dB in the case of the 5 m- and 7 m-long EYDF, respectively). These results, obtained via simulations, are used as a baseline to select the EYDF length and pump

power for the experimental setup. Accordingly, the first laboratory test was performed using a 7 m-long EYDF span pumped with 3 W. The obtained experimental results show a narrower and flatter EYDFA gain profile compared to the simulations; it is shifted towards longer wavelengths and has a steep drop below 1544 nm. Hence, the 7 m-long EYDF is too long for the chosen application; therefore, the measurements are repeated using shorter EYDF spans (5 m, 3 m, and 2 m) to determine a more appropriate length.

The comparison between the experimental and simulation results is shown in Figure 9. The closest match is in the case of the 3 m-long EYDF in the wavelength range of 1545–1560 nm. Experimental data for longer (5 m and 7 m) EYDF sections shows the appearance of signal reabsorption in the spectral range 1530–1540 nm that coincides with the Er^{3+} maximum absorption (see Figure 4). This results in additional signal gain around 1560 nm. It is evident that signal reabsorption has not been taken into account by our simulation model to the required degree. Simulations and experimental data mismatch (especially for 2 m) may be related to the specific shape of the EYDF's inner cladding (and its pump-focusing properties), which is represented in a simplified form in the simulation model as a coefficient (overlap factor). Although simulation data cannot be used to accurately describe the gain shape, these data are useful for determining the initial values of the laboratory setup.

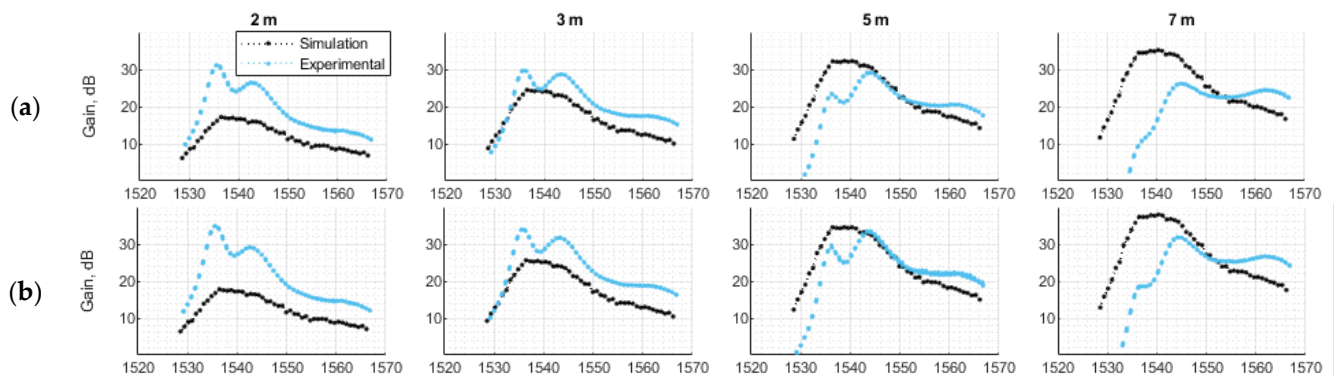


Figure 9. Experimental EYDFA gain measurements overlaid on simulation results at -20 dBm/ch signal power and a pump power of (a) 1 W and (b) 2 W.

The per-channel gain of the EYDFA setup is analyzed using a 48-channel dummy WDM signal constructed using the wideband ASE noise source and WSS (as described in Section 3). After filtering, the signal power level is adjusted with a variable optical attenuator. Note that the number of DWDM channels/wavelengths is limited by the operating band of the WSS. The gain spectra of the cladding-pumped EYDFA are captured for the configurations with the EYDF span lengths of 2 m, 3 m, 5 m, and 7 m, while the signal input power is kept constant at -25 dBm/ch, -20 dBm/ch, and -10 dBm/ch (see Figure 10).

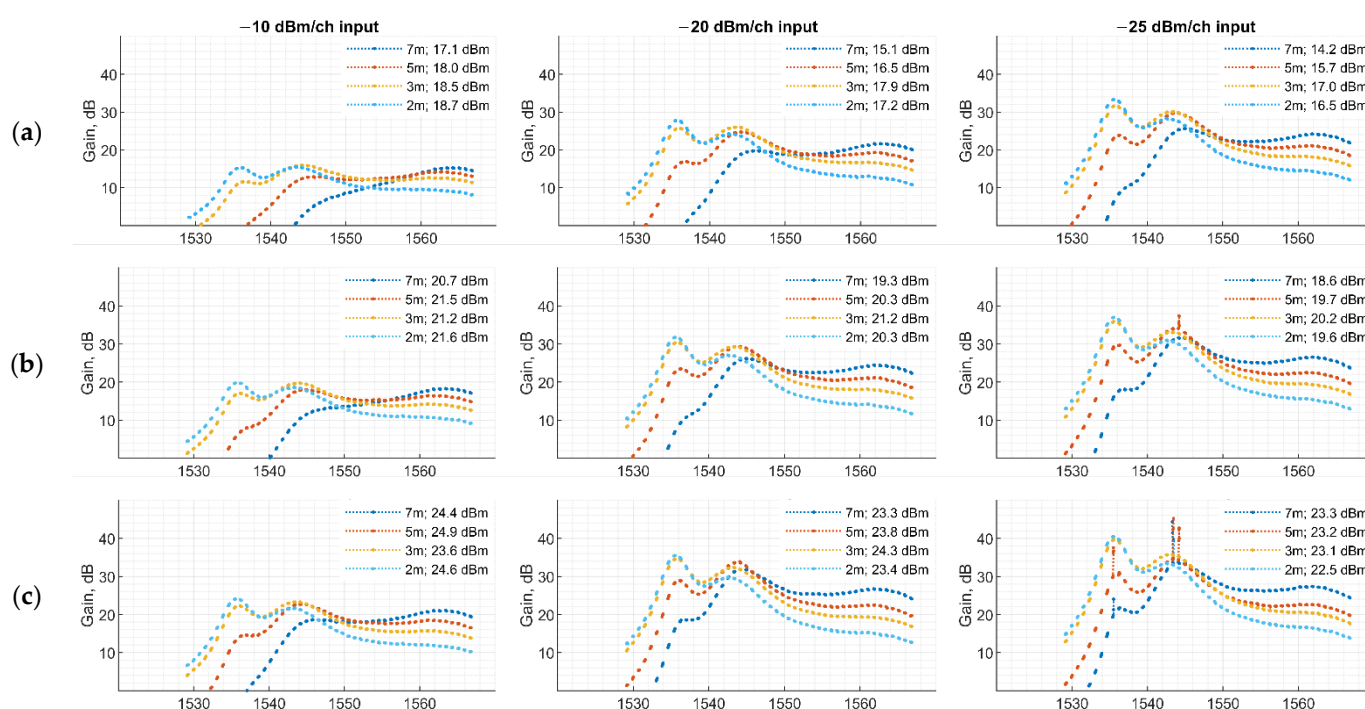


Figure 10. Experimentally determined EYDFA gain at three different input signal powers vs. EYDF length and pump power of (a) 0.6 W, (b) 1 W, (c) 2 W. Legend on each graph shows fiber length and total output power.

We observed undesirable lasing peaks at pump power above 1 W for the cases with the signal input power of -25 dBm/ch. At the highest signal input power level (-10 dBm/ch), the amplifier’s usable bandwidth shifts towards longer wavelengths as the EYDF length increases. At the lowest signal input power level (-25 dBm/ch) when increasing the EYDF length from 2 m to 5 m, the power levels of channels at 1544 nm remain almost unchanged (less than 1 dB difference), whereas the longer wavelengths experience significantly higher gain. If the EYDF length is further increased from 5 m to 7 m, channels with wavelengths above 1544 nm are amplified even more. However, the gain is decreased by 10 dB for channels at around 1536 nm and a rapid drop-off was seen below 1536 nm. Such amplification is explained by the Er^{3+} population inversion. Specifically, the high population inversion [27] of Er^{3+} required for the amplification at these wavelengths was not maintained throughout such a long EYDF span, which results in the non-uniformity of the gain spectra. Additionally, we observed that the first meter of the EYDF glows in green when the pump source is active (shown in Figure 11). This glow originates from the Er^{3+} upconversion luminescence, indicating a high population inversion. The effect diminishes when the input signal is coupled into the EYDFA for the amplification as some of the excited Er^{3+} return to the ground state by amplifying our C band signal.

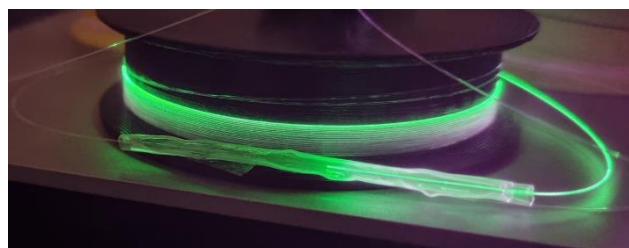


Figure 11. Green luminescence of the EYDF while pump is active. A purple tinge is also visible due to some pump light leaking from the fiber that is picked up by the camera. The fusion splice protection sleeve had its steel rod removed to avoid potential thermal expansion effects.

Figure 12 shows that, regardless of the signal input power, a portion of the pump power that is absorbed by the 5 m EYDF span increases only by 0.5 dB, even when the pump power is increased from 0.6 W to 2.5 W and then further to 3.5 W.

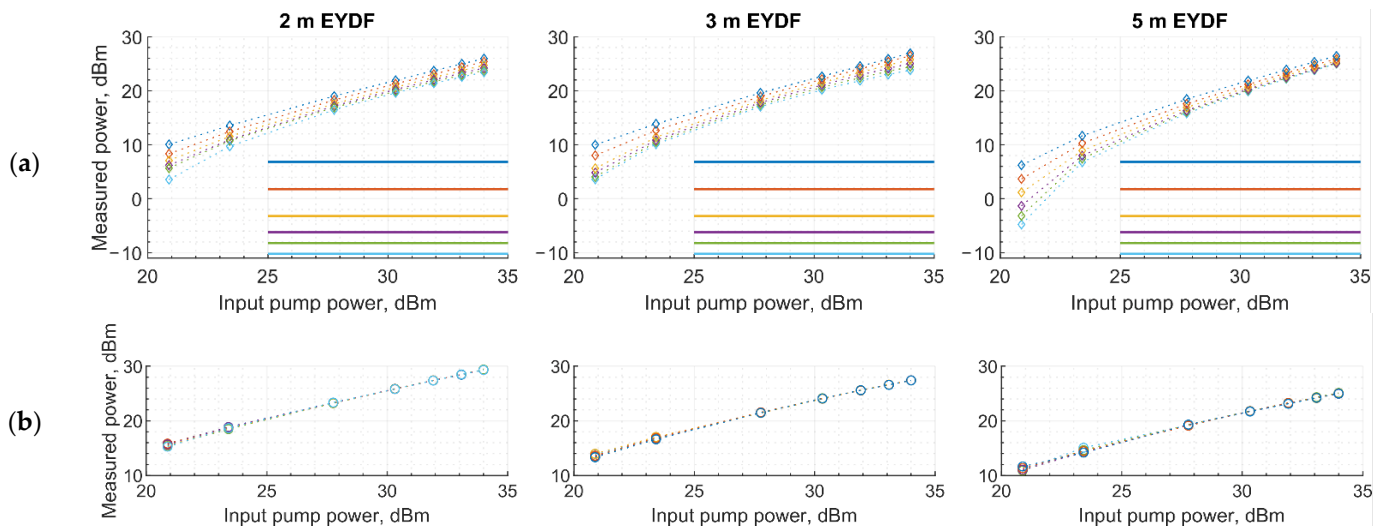


Figure 12. Measured power for (a) output signal and (b) residual pump coming out of the EYDF. Horizontal lines indicate total input signal power and correspond to -10 (top), -15 , -20 , -23 , -25 , -27 (bottom) dBm per channel.

For the 2 m EYDF, the pump power absorption remains nearly constant. A slight mismatch at low pump powers is explained by the instability of the output power when the pump diode is biased slightly below or at its specified minimum threshold current. For any given operational pump power, the major portion of the signal amplification is achieved within the first few EYDF meters, having reached a point of power saturation. Total output power increases only by 1 dB when the fiber length is increased from 2 m to 5 m. The signal output power is not strongly dependent on its input power, even for levels above those reasonably expected in telecom links. Given the absorption peak at 1536 nm, longer EYDF spans cannot be used for the wavelength channel transmission at these lower wavelengths as the signal loss is not sufficiently counteracted by the gain in this part of the spectra. The longer the EYDF length, the more the lower wavelengths are absorbed and the more their power is redistributed to longer wavelengths, effectively shifting the usable bandwidth towards the far end of the optical C-band.

5. Conclusions

In this paper, we show the process of designing an inhouse cladding-pumped EYDFA prototype using numerical simulations and experimental characterization. We identified the EYDFA configuration (a co-doped fiber length, pump power, input signal power) suitable for the signal amplification in a multichannel fiber-optic transmission system with dense wavelength allocation across the C-band. For the EYDFA, we used a commercial double-clad EYDF as an active medium. Therefore, we first experimentally determined the EYDF characteristics (specifically, Er^{3+} and Yb^{3+} absorption and emission cross-sections and overlap coefficients). Then, these were fed into a simulation model to determine some initial EYDFA settings, e.g., the EYDFA length and the pump power required to ensure the desired amplification, before moving to a laboratory setup. Finally, we used the developed prototype to investigate the EYDFA’s absolute gain and gain uniformity under different conditions using a 48-channel DWDM system with -20 dBm/ch. input power. The obtained results reveal that the EYDFA setup, consisting of a 5 m-long EYDF span that is optically pumped by a multimode diode with 2 W pump power, ensures practical levels of amplification in the 1534–1565 nm band. Across this wavelength range, the

EYDFA provides >21 dB per-channel gain with 12 dB gain ripple when amplifying 48 channels at 100 GHz spacing.

For pump powers up to 2 W, the population inversion of Er³⁺ required for signal amplification in the wavelength region below 1544 nm is not maintained throughout EYDF spans longer than 5 m. This causes a gain increase in the upper C-band, which occurs due to signal reabsorption from the lower C-band. Furthermore, during the EYDFA characterization, we observed unstable lasing for the EYDFA configurations when combining high pump power and low input signal power. For the input signal power below −20 dBm/ch, the EYDFA generated some lasing modes even when the pump power was as low as 0.6 W. Two peaks were distinguished at 1536 and 1544 nm. The intensity of those peaks is proportional to the EYDF length; however, such behavior can be eliminated by increasing the power of the input C-band signal.

Author Contributions: Conceptualization, K.Z., A.S., S.S., O.O., J.G., V.B.; methodology, K.Z., A.U., A.S., S.O., J.G.; validation, K.Z., A.S., J.G.; formal analysis, A.U. A.S., S.O., I.L., J.G., L.B.; investigation, K.Z., A.U., D.P., A.S., S.S., O.O., S.O., I.L., J.G., L.B.; data curation, K.Z., A.U., A.S., S.O., J.G.; writing—original draft preparation, K.Z., A.U., A.S., S.S., S.O., I.L., J.G., L.B.; writing—review and editing, K.Z., A.U., A.S., O.O., J.G.; visualization, K.Z., S.O., I.L., J.G., L.B.; supervision, A.S., S.S., J.G., V.B.; project administration, A.S., S.S., J.G., V.B. All authors have read and agreed to the published version of the manuscript.

Funding: This work is supported by the European Regional Development Fund project No. 1.1.1.1/18/A/068.

Institutional Review Board Statement: Not applicable.

Informed Consent Statement: Not applicable.

Data Availability Statement: The data that supports the findings of this study are available within the article.

Acknowledgments: The Institute of Solid State Physics, University of Latvia, as a Center of Excellence, has received funding from the European Union's Horizon 2020 Framework Programme H2020-WIDESPREAD-01-2016-2017-TeamingPhase2 under grant agreement No. 739508, project CAMART2. We express our gratitude to rer. nat. Nicoletta Haarlammer from Fraunhofer Institute for Applied Optics and Precision Engineering IOF for the refractive index measurements of ytterbium/erbium-co-doped fibers.

Conflicts of Interest: The authors declare no conflict of interest.

References

1. Peterka, P.; Koška, P.; Jasim, A.A.; Kanagaraj, N.; Aubrecht, J.; Kamrádek, M.; Podrazký, O.; Todorov, F.; Kašík, I.; Honzátko, P. Enhanced Pump Absorption Efficiency in Coiled and Twisted Double-Clad Fibers for Fiber Lasers. In Proceedings of the 2019 21st International Conference on Transparent Optical Networks (ICTON), 9–13 July 2019; pp. 1–4. <https://doi.org/10.1109/ICTON.2019.8840274>.
2. Andrianov, A.V.; Skobelev, S.A.; Balakin, A.A.; Anashkina, E.A.; Litvak, A.G. Tapered Multicore Fiber for High-Power Laser Amplifiers. *IEEE Photonics J.* **2022**, *14*, 1505606. <https://doi.org/10.1109/JPHOT.2021.3135349>.
3. Anashkina, E.A.; Andrianov, A.V. Design and Dispersion Control of Microstructured Multicore Tellurite Glass Fibers with In-Phase and Out-of-Phase Supermodes. *Photonics* **2021**, *8*, 113. <https://doi.org/10.3390/photonics8040113>.
4. Marisova, M.P.; Andrianov, A.V.; Leuchs, G.; Anashkina, E.A. Dispersion Tailoring and Four-Wave Mixing in Silica Microspheres with Germanosilicate Coating. *Photonics* **2021**, *8*, 473. <https://doi.org/10.3390/photonics8110473>.
5. Supe, A.; Olonkins, S.; Udalcovs, A.; Senkans, U.; Mūrnieks, R.; Gegere, L.; Prigunovs, D.; Grube, J.; Elsts, E.; Spolitis, S.; et al. Cladding-Pumped Erbium/Ytterbium Co-Doped Fiber Amplifier for C-Band Operation in Optical Networks. *Appl. Sci.* **2021**, *11*, 1702. <https://doi.org/10.3390/app11041702>.
6. Matte-Breton, C.; Ryf, R.; Fontaine, N.K.; Essiambre, R.-J.; Chen, H.; Kelly, C.; Messaddeq, Y.; LaRochelle, S. Modeling and Characterization of Cladding-Pumped Erbium-Ytterbium Co-Doped Fibers for Amplification in Communication Systems. *J. Lightwave Technol.* **2020**, *38*, 1936–1944. <https://doi.org/10.1109/JLT.2019.2961061>.
7. Al-Azzawi, A.A.; Almukhtar, A.A.; Reddy, P.H.; Dutta, D.; Das, S.; Dhar, A.; Paul, M.C.; Zakaria, U.N.; Ahmad, H.; Harun, S.W. Compact and Flat-Gain Fiber Optical Amplifier with Hafnia-Bismuth-Erbium Co-Doped Fiber. *Optik* **2018**, *170*, 56–60. <https://doi.org/10.1016/j.ijleo.2018.05.104>.

8. Miluski, P.; Kochanowicz, M.; Żmojda, J.; Dorosz, D.; Łodziński, M.; Baranowska, A.; Dorosz, J. Eye Safe Emission in Tm³⁺/Ho³⁺ and Yb³⁺/Tm³⁺ Co-Doped Optical Fibers Fabricated Using MCVD-CDS System. *Opt. Mater.* **2020**, *101*, 109711. <https://doi.org/10.1016/j.optmat.2020.109711>.
9. Pathfinder™ X-ray Microanalysis Software. Available online: <https://www.thermofisher.com/order/catalog/product/IQLAADGABKFAQOMBJE> (accessed on 20 January 2022).
10. Várallyay, Z.; Szabó, Á.; Rosales, A.; Gonzales, E.; Tobioka, H.; Headley, C. Accurate Modeling of Cladding Pumped, Star-Shaped, Yb-Doped Fiber Amplifiers. *Opt. Fiber Technol.* **2015**, *21*, 180–186. <https://doi.org/10.1016/j.yofte.2014.11.003>.
11. Jeong, Y.; Sahu, J.K.; Payne, D.N.; Nilsson, J. Ytterbium-Doped Large-Core Fiber Laser with 1.36 KW Continuous-Wave Output Power. *Opt. Express OE* **2004**, *12*, 6088–6092. <https://doi.org/10.1364/OPEX.12.006088>.
12. Supe, A.; Spolitis, S.; Elsts, E.; Murnieks, R.; Doke, G.; Senkans, U.; Matsenko, S.; Grube, J.; Bobrovs, V. Recent Developments in Cladding-Pumped Doped Fiber Amplifiers for Telecommunications Systems. In Proceedings of the 2020 22nd International Conference on Transparent Optical Networks (ICTON), 19–23 July 2020; pp. 1–6. <https://doi.org/10.1109/ICTON51198.2020.9203436>.
13. Eclipse LV150N and LV150NA|Upright Microscopes|Nikon Metrology. Available online: <https://www.nikonmetrology.com/en-gb/industrial-microscopes/upright-microscopes-eclipse-lv150n-and-lv150na> (accessed on 16 December 2021).
14. Nikon|Industrial Metrology|Objectives for Industrial Microscopes. Available online: <https://www.nikon.com/products/industrial-metrology/lineup/microscope/industrial-microscopes/accessory/objective/> (accessed on 16 December 2021).
15. DS-Fi3|Digital Sight Cameras|Nikon Metrology. Available online: <https://www.nikonmetrology.com/en-gb/industrial-microscopes/digital-sight-cameras-ds-fi3> (accessed on 16 December 2021).
16. Lee, S.W.; Lee, S.Y.; Pahk, H.J. Precise Edge Detection Method Using Sigmoid Function in Blurry and Noisy Image for TFT-LCD 2D Critical Dimension Measurement. *Curr. Opt. Photon., COPP* **2018**, *2*, 69–78.
17. Ma, H.-P.; Yang, J.-H.; Yang, J.-G.; Zhu, L.-Y.; Huang, W.; Yuan, G.-J.; Feng, J.-J.; Jen, T.-C.; Lu, H.-L. Systematic Study of the SiO_x Film with Different Stoichiometry by Plasma-Enhanced Atomic Layer Deposition and Its Application in SiO_x/SiO₂ Super-Lattice. *Nanomaterials* **2019**, *9*, 55. <https://doi.org/10.3390/nano9010055>.
18. Multi-Angle Absolute Specular Reflectance, Cary UMA|Agilent. Available online: <https://www.agilent.com/en/product/molecular-spectroscopy/uv-vis-uv-vis-nir-spectroscopy/uv-vis-uv-vis-nir-accessories/cary-universal-measurement-accessory-uma> (accessed on 16 December 2021).
19. RonD FiberMate2™ Fiber Optic Coupler. Available online: <https://www.harricksci.com/ftir/accessories/group/Fiber-Mate2%E2%84%A2-Fiber-Optic-Coupler> (accessed on 16 December 2021).
20. Huang, F.; Liu, X.; Ma, Y.; Kang, S.; Hu, L.; Chen, D. Origin of near to Middle Infrared Luminescence and Energy Transfer Process of Er³⁺/Yb³⁺-co-Doped Fluorotellurite Glasses under Different Excitations. *Sci. Rep.* **2015**, *5*, 8233. <https://doi.org/10.1038/srep08233>.
21. McCumber, D.E. Einstein Relations Connecting Broadband Emission and Absorption Spectra. *Phys. Rev.* **1964**, *136*, A954–A957. <https://doi.org/10.1103/PhysRev.136.A954>.
22. VPIphotonics Design Suite™—Overview. Available online: <https://www.vpi-photonics.com/Tools/DesignSuite/> (accessed on 16 December 2021).
23. VPIphotonics GmbH. *VPIcomponentMaker Fiber Optics User's Manual*; VPIphotonics GmbH: Berlin, Germany, 2020; pp. 176–204.
24. VPIphotonics GmbH. *VPIcomponentMaker Fiber Optics Module Reference*; VPIphotonics GmbH: Berlin, Germany, 2020.
25. Meng, Q.; Li, J.; Wu, H.; Han, B.; Wang, Z. Cladding-Pumped Erbium-Ytterbium Co-Doped Random Fiber Laser. In Proceedings of the 2017 16th International Conference on Optical Communications and Networks (ICOON), 7–10 August 2017; pp. 1–2. <https://doi.org/10.1109/ICOON.2017.8121303>.
26. Meng, Q.; Wu, H.; Han, B.; Li, J.; Wang, Z. LD-Pumped Random Fiber Laser Based on Erbium-Ytterbium Co-Doped Fiber. *Photonic Sens.* **2020**, *10*, 181–185. <https://doi.org/10.1007/s13320-019-0553-x>.
27. Bai, X.; Wang, M.; Yang, Y.; Liu, Z.; Jia, W. Experimental and Theoretical Analysis on Pump Spectral Propriety of Single Frequency Erbium-Ytterbium Co-Doped Fiber Amplifier. *J. Phys. Commun.* **2021**, *5*, 015005. <https://doi.org/10.1088/2399-6528/abd8ec>.